JOURNAL OF CATALYSIS 145, 551–560 (1994)

Kinetic Studies of the Isomerization of *n*-Butenes over Boroaluminosilicate Zeolites

Daniel Bianchi,*,[1] Mark W. Simon,† Sang Sung Nam,† Wen-qing Xu,† Steven L. Suib,*,†,‡,[2] and Chi-Lin O'Young§,[2]

*Department of Chemical Engineering, †U-60, Department of Chemistry, and ‡Institute of Materials Science, University of Connecticut, Storrs, Connecticut 06269-3060; and §Texaco, Inc., P.O. Box 509, Beacon, New York 12508

Received June 4, 1993; revised September 9, 1993

Boroaluminosilicate zeolites have been used as *n*-butene isomerization catalysts in this study. Al^{3+} free boron zeolites are inactive for *n*-butene isomerization. Spectroscopic and microscopic studies have been used to monitor the structure, thermal stability, and acidity of these materials. Kinetic studies are the main focus of this paper, with an emphasis on determination of the mechanism of *n*-butene isomerization over boron zeolites. Results show that the reaction is first order in *n*-butenes with slow deactivation via coke formation. Isobutylene, propylene, and C_5–C_8 polymeric species are the main products. Comparisons of the activity and selectivity of boroaluminosilicates, Al^{3+}-free B zeolites, and Al^{3+} is necessary to enhance yields of isobutylene. A two-step model is proposed to account for product selectivity, deactivation, and observed kinetic data. © 1994 Academic Press, Inc.

INTRODUCTION

There is considerable recent interest in the production of isobutylene (i-C_4H_8) from its isomers due to its use in production of methyl *tert*-butyl ether (MTBE) which has a high octane number (115-135), and is used as a gasoline additive, and in the production of isoprene and methacrylic acid which are used in polymer synthesis (1).

Environmental concerns have led to synthetic efforts to form less volatile commercially useful products such as isobutylene. Fluorinated Al_2O_3 catalysts have been used for *n*-butene isomerization (2, 3), however, such catalysts cannot suppress polymerization reactions.

Zeolites (4–6) have been used in reactions of *n*-butenes with formation of light hydrocarbons, gasoline, diesel range hydrocarbons, and, in particular, aromatics. Recently, Thomas (7) has suggested that 10 member ring zeolites would be useful in the transformation of *n*-butenes to isobutylene.

Isomorphous substitution of ions in zeolite frameworks has recently been a major area of research (8–10). Specific emphasis has been on the incorporation of Fe^{3+}, B^{3+}, and Ga^{3+}, particularly in ZSM-5 type materials (11–13). Acidic properties of resultant materials are significantly modified from Al^{3+}-containing zeolites (14–19). Synthesis and characterization of these systems has been a major focus (20–24), although sorption and catalytic properties have also been reported (14, 16–19, 22, 25, 26).

In the case of B^{3+} substitution in zeolites, weak acidity has been observed (14–19) for these materials. Reactions catalyzed by B^{3+} zeolites include isomerization of xylene (16, 18), *n*-decane isomerization and hydrocracking (9), dehydration of alcohols (16, 24), dealkylation (16), alkylation (17, 22, 25), toluene disproportionation (17, 26), *n*-hexane cracking (16), catalytic dewaxing (18), hexene isomerization (27), pentane hydroisomerization (28), and cyclopropane isomerization (16). Catalytic activity in these systems was often linked to trace amounts of Al^{3+} in the zeolite and not to the B^{3+} content or B^{3+} sites (16, 20).

Both B–ZSM-5 and B–ZSM-11 with low levels of Al^{3+} ions have weak acidity and are thermally stable in air to about 900°C (29). Luminescence, ^{11}B NMR, Fourier transform infrared, and temperature-programmed desorption studies were used to monitor the local B^{3+} environment in the zeolite, migration of boron to the surface of the zeolite and trends in acidity and stability as a function of boron content. Ab initio calculations have also been used to study acidic properties of boron zeolites (30).

This paper concerns the isomerization of *n*-butenes to isobutylene over boroaluminosilicates, Al^{3+}-free borosilicates, and Al^{3+}-containing ZSM-5, ZSM-11, and BETA zeolites. The objective of the work is to study the mechanism, deactivation, and regeneration of boron zeolite catalysts.

[1] Present address: Lab. Thermodynamique et cinetique chimiques, Laboratoire associé au CNRS#231, Université Claude Bernard, Poste 35.54 Villeurbanne, France.

[2] To whom correspondence should be addressed.

0021-9517/94 $6.00

II. EXPERIMENTAL

A. Catalytic Reactor System

The isomerization of *n*-butenes to isobutylene has been studied in a stainless-steel continuously stirred tank reactor (CSTR) of 1.5 cm^3 volume as has been described previously (31). The weight of the powdered catalyst is in the range of 0.1 to 0.3 g and supported on glass wool. The gas flow control system was operated at 1 atm total pressure to give flows in the range of 5 to 500 cm^3/min which permits work under differential reactor conditions (conversion <10%). In some experiments, water is introduced into the reactive mixture using a saturator.

The composition of the gas mixture at the outlet of the reactor is studied with gas chromatography (GC) with a flame ionization detector. The separation of hydrocarbons is obtained using a GasCHROM C8 column at either a constant temperature (40°C) for paraffins and olefins up to C4 (except unresolved C_2H_4 and C_2H_6) or with temperature programming (up to 110°C) for heavier hydrocarbons. The compounds identified at the outlet of the reactor are CH_4, (C_2H_4 or C_2H_6), C_3H_8, C_3H_6, iso-C_4H_{10}, *n*-C_4H_{10}, 1-butene, isobutylene, *t*-2-butene and *c*-2-butene with numerous heavier products (30 peaks) detected at lower concentrations when using temperature programming. Isobutylene is the primary product with propylene as the main secondary product of the reaction with its concentration increasing with conversion (vide infra).

As an example, the composition of the gas mixture at the outlet of the reactor for 20% 1-butene feed at a high conversion for a reaction temperature of 523°C is CH_4 = 0.15%, C_2H_4 or C_2H_6 = 0.4%, C_3H_8 = 0.05%, C_3H_6 = 3.3%, iso-C_4H_{10} = 0.15%, *n*-C_4H_{10} = 0.02%, 1-butene = 2.4%, isobutylene = 5.9%, *t*-2-butene = 3.3%, and *c*-2-butene = 2.5%. The other 30 products have not been quantified but the total area of their peaks from GC studies represents about 2% of the total area for all peaks. A GC mass spectrometry (MS) study showed that compounds having masses as high as 250 corresponding to C_{17}–C_{20} compounds were formed. The formation of aromatic compounds from *n*-butenes over zeolites (ZSM-5) has been observed by Ono *et al.* (32).

For some experiments the outlet of the reactor was connected to a Nuclide magnetic sector mass spectrometer for continuous quantitative analysis of specific gases. For example, deactivation of the catalyst is observed with time on stream. Regeneration of the catalyst is obtained using either hydrogen or oxygen treatment (vide infra). With the mass spectrometer, the rate of production of CH_4 is recorded continuously (peak *m/e* = 15) during H_2 treatment. For O_2 treatment, the rate of production of CO_2 is recorded using the peak with *m/e* = 44. A diagram of the reactor is shown in Fig. 1.

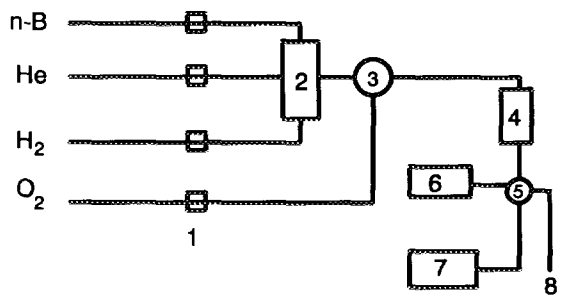

FIG. 1. Diagram of reactor and apparatus: (1) flow valves, (2) rotameter, (3) three-way valve, (4) reactor, (5) 4 way valve, (6) GC, (7) MS, and (8) vent.

B. Catalyst Treatment before Reaction

The solids are dehydrated and activated at 520°C under argon flow (30 cm^3/min). The temperature is increased at 50°C/h from room temperature to 350°C and then at 100°C/h until final temperature (4 h treatment at final temperature.

C. Synthesis of Catalysts

Boron containing zeolites ZSM-5 [B/Al–ZSM-5] and ZSM-11 [B/Al–ZSM-11] containing low levels of Al^{3+} ions were prepared according to procedures discussed elsewhere (29). In some cases, Al^{3+}-free B–ZSM-11 [B–ZSM-11] catalysts were prepared by mixing boric acid and tetrabutylammonium hydroxide at pH 13 in NH_4OH and tetraethylorthosilicate to form a sol. This sol was heated at 170°C in an autoclave for 5 days. At times tetrabutylammonium iodide salts were used instead of TBAOH. Al^{3+}-free B–ZSM-5 zeolites [B–ZSM-5] were also prepared in a similar manner by using tetrabutylammonium bromide (33). For some experiments, boron-BETA zeolite [B/Al-BETA] was prepared according to procedures described in the literature (34).

D. Morphology Studies

Scanning electron microscopy (SEM) experiments were done on an AMRAY 1810 D scanning electron microscope with an AMRAY PV9800 energy dispersive X-ray (EDX) analyzer.

E. Infrared Experiments

Fourier transform infrared (FTIR) experiments were done on a Mattson Galaxy spectrometer having a resolution of 2 cm^{-1} by using either self supporting wafers or KBr pellets and a triglycine sulfate detector. Pyridine chemisorption experiments were done with self supporting wafers in a home-built *in situ* cell by first dehydrating the zeolite to a desirable temperature (typically 380°C) followed by sorption of pyridine at room temperature.

TABLE 1

Synthetic and Analytic Data for Catalysts[a]

Catalyst	[B][b]	[Al][c]	Si source[d]
B-ZSM-5	0.40	<1	TEOS
B-ZSM-11	0.25	<1	TEOS
B-Beta	0.85	<1	TEOS
B/Al-ZSM-5	0.52	200–300	Ludox
B/Al-ZSM-11	0.25	200–300	Ludox
B/Al-Beta	1.24	200–300	Ludox

[a] [B] and [Al] determined by atomic absorption methods.
[b] In wt%.
[c] In parts per million.
[d] TEOS, tetraethylorthosilicate.

Samples were evacuated at 1×10^{-5} Torr overnight to remove physisorbed pyridine.

F. Ammonia Desorption

Ammonia sorption and desorption experiments were done on a home-built reactor system consisting of a gas chromatograph detector, a tube furnace, a temperature programmer, an integrator, and a stainless-steel reactor. Linear temperature program rates are used in these experiments. Samples were first dehydrated *in situ* in He at 500°C for 1 h, then cooled to 100°C in He, then ammonia was sorbed at 100°C, then physisorbed ammonia was removed with flowing He at 100°C overnight for sorption experiments. Temperature programming in He gas was then carried out.

III. RESULTS

A. Synthesis

Synthesis of Al^{3+}-free B–ZSM-5 and B–ZSM-11 crystals was verified by X-ray powder diffraction, atomic absorption, and energy dispersive X-ray analyses. X-ray powder diffraction patterns consistent with the desired B–ZSM-5 or B–ZSM-11 phases were obtained. Unit cell volume for B-ZSM-5 with no Al^{3+} is 5304 and 5343 Å^3 for B–ZSM-11. Al^{3+} content was consistent with levels below 1 ppm from atomic absorption experiments. Crystallographic diffraction patterns for boron-BETA zeolite were obtained that are consistent with the BETA structure. Compositions of all B-containing materials reported throughout this paper are given in Table 1 along with B and Al contents determined from atomic absorption experiments.

B. Morphology

The morphology of Al^{3+}-free B–ZSM-11 crystals was markedly different than materials containing 300 ppm Al^{3+} [B/Al–ZSM-11] materials as described in earlier research (29). An SEM photo of an Al^{3+}-free B–ZSM-5 crystallite having a rice shape and a length of about 2 μm and a width of about 1 μm is shown in Fig. 2. A corresponding energy dispersive X-ray analysis for this material is given in Fig. 3.

C. Infrared Spectroscopy

Infrared spectra for B/Al–ZSM-5 dehydrated at 700, 800, and 900°C are shown in Fig. 4. Bands at 1383 and 961 cm^{-1} are observed for this material. Similar bands at 1384 and 933 cm^{-1} are observed for B/Al–ZSM-11. Pyridine chemisorption experiments with FTIR detection show the presence of both Lewis and Brönsted sites in all of these boroaluminosilicate materials, including B/Al–ZSM-5, B/Al–ZSM-11, and B/Al-BETA.

D. Ammonia Desorption

Ammonia TPD Data for B/Al–ZSM-11 for different calcination temperature treatments are shown in Fig. 5. The number of micromoles of ammonia decreases almost in a linear manner as calcination temperature is increased from 600°C to 900°C.

E. Kinetic Results

The major goal of this research is to determine the experimental conditions to be used for selective conversion of *n*-butenes to isobutylene over boroaluminosilicate zeolite catalysts. The conversion of *n*-butenes (1-butene, B1; *c*-2-butene, B2C; and *t*-2-butene, B2T) to isobutylene (I) on Al^{3+}-free materials (B–ZSM-5, B–ZSM-11, and B-BETA) has not been detected in the range $T < 530$°C. At these temperatures over borosilicate materials, only interconversion of *n*-butenes is observed. All other studies reported here are for boroaluminosilicate zeolites (29) containing some Al^{3+} (300–800 ppm). Earlier reports suggest that trace levels of Al^{3+} are responsible for acid-catalyzed reactions (16, 20).

For boroaluminosilicate solids studied here, interconversion of *n*-butenes is observed even at room temperature. Starting with B1 (20% B1/He) as reactant, the initial selectivity at room temperature for a conversion of 2% B1 is B2C/B2T = 1.4, a value higher than the thermodynamic ratio. Deactivation with time on stream (TOS) is observed. Others have studied the conversion of B1 to B2C and B2T (35) in great detail. These reactions are first order as on classic oxide catalysts like SiO_2 and Al_2O_3 (36) and global reversible kinetic models (35) have been proposed as depicted below:

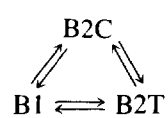

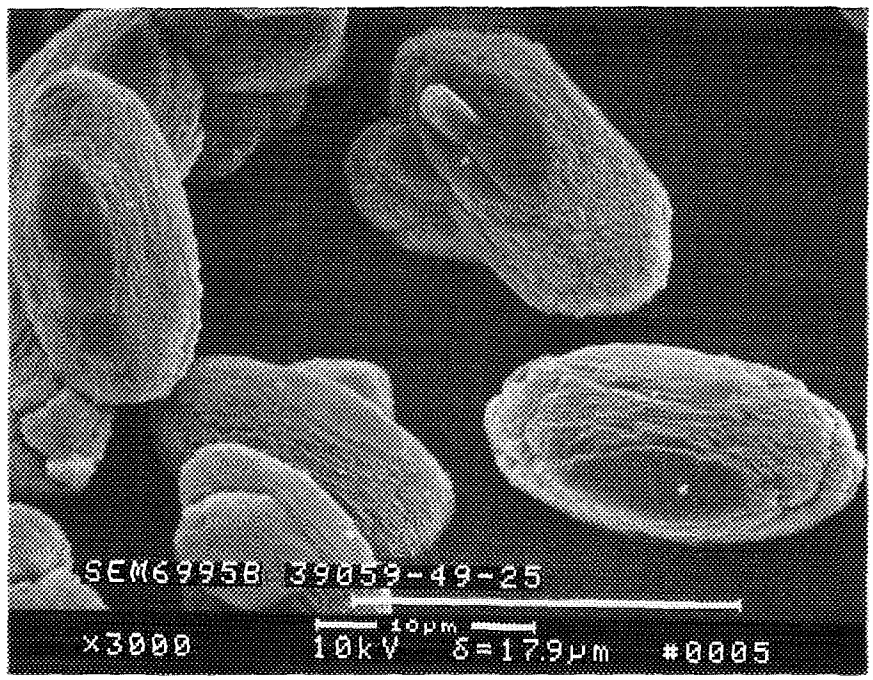

FIG. 2. Scanning electron micrograph of Al^{3+}-free B-ZSM-11.

The activation energy for the isomerization of B1 has been found to be about 55–63 kJ/mol for various zeolites (35). Therefore, at the high temperatures needed for formation of I ($T > 400$°C) even with a high space velocity the conversion of B1 to B2C and B2T will be high. In fact, the thermodynamic ratio for normal butenes here is almost obtained. For example, the thermodynamic mole fractions x_i (i = 1, B1; i = 2, B2C; and i = 3, B2T) at 523°C are $x_1 = 0.213$, $x_2 = 0.30$, and $x_3 = 0.445$ [using thermodynamic data from (37)]. At the same temperature using 20% B1/He, the composition of normal isomers is $x_1 = 0.30$, $x_2 = 0.30$, and $x_3 = 0.31$ for a conversion of n-butenes to isobutylene of 10%. These values are close to the thermodynamic equilibrium for n-butenes (38). Therefore, only the conversion of n-butenes (B) to I is discussed here.

F. *Deactivation Effect*

Figure 6 shows $\partial I/\partial t$ at 523°C vs TOS for a 20% B1/He feed, a mass of B/Al-BETA catalyst of 0.115 g, a flow rate of 20 cm^3/min, and a conversion of 5%. The B/Al-BETA catalyst deactivates slowly at this temperature and a real steady state is never obtained even after several

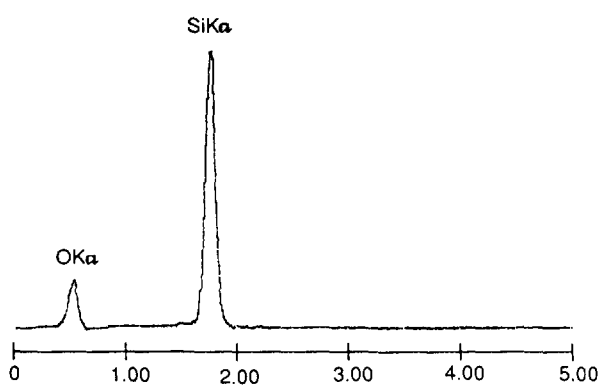

FIG. 3. Energy dispersive X-ray analysis of Al^{3+}-free B-ZSM-11.

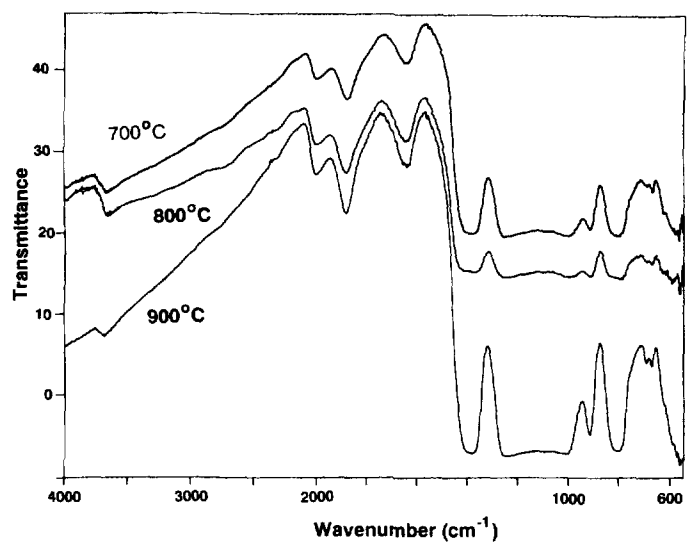

FIG. 4. FTIR spectra of B/Al-ZSM-5 Calcined at 700, 800, and 900°C.

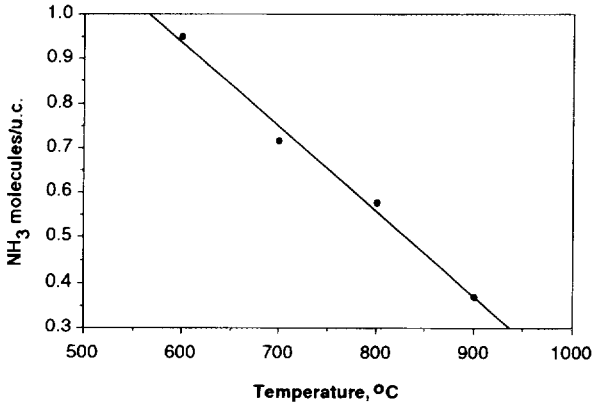

FIG. 5. Plot of micromoles ammonia vs calcination temperature (°C) for B/Al–ZSM-11 (0.28 wt% B).

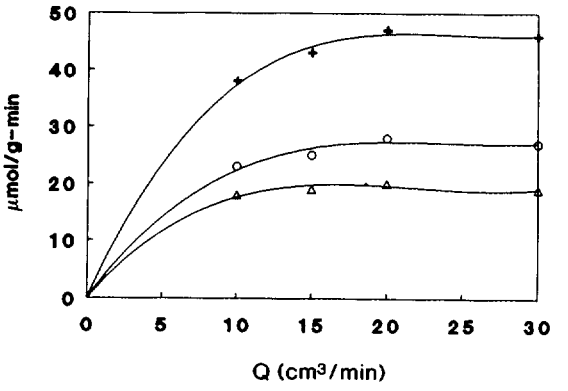

FIG. 7. Plot of activity (μmol/g · min) vs flow rate for B/Al-BETA zeolite: (△) 440°C, (○) 523°C, and (+) 502°C.

hours. A slow accumulation of by-products occurs continuously. If the temperature of reaction is increased the rate of deactivation is higher. This general effect is observed for all boroaluminosilicate catalysts that have been studied in our laboratories.

G. *Diffusion Effects*

1. External diffusion. External diffusion effects have been studied for low conversion values for *n*-butenes (<5%), under differential reactor conditions. Figure 7 shows the rate of I formation as a function of flow rate for three temperatures of reaction, using a mass of B/Al-BETA catalyst of 0.12 g. A constant rate is obtained only for flow rates >18 cm^3/min because at lower flow rates, external diffusion influences the rate of production of *I* (39a). In order to avoid external diffusion control, flow rates >18 cm^3/min were always used. Note that these two curves can not be used to determine the activation energy of reaction because (due to continuous deactivation of the catalyst) activities can not be measured for the same surface densities of sites. The data at 532°C represent a B/Al-BETA catalyst that has already been used for several hours longer than the data at 502°C, however, activity is significantly lower. Similar trends were observed for B/Al–ZSM-5 and B/Al–ZSM-11.

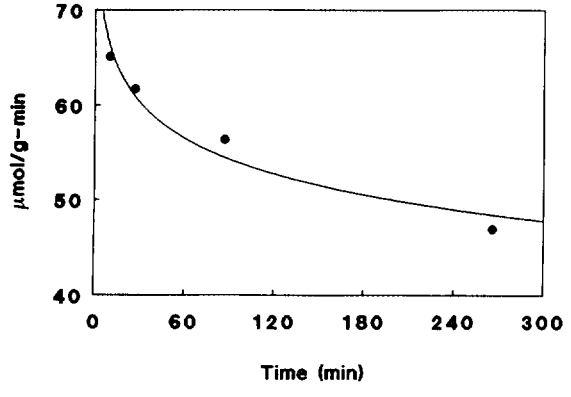

FIG. 6. Plot of activity (μmol/g · min) for isobutylene formation vs time in min, B/Al-BETA catalyst, 523°C, 5% conversion.

2. Intraparticle diffusion. The effects of intraparticle diffusion can only be estimated since it is difficult to produce zeolites of controlled particle size, especially for zeolites having different amounts of B and Al and different pore sizes. Crushing the initial particles (average diameter 2 μm, see Section IV.B) to obtain particles of smaller sizes may change the morphology of the particles and catalytic sites.

Using the classical formula (39a)

$$\Phi_s = R_p^2\,(r)/D_{eff}\,c \qquad [1]$$

and considering the value of the various parameters, R_p the radius of the particles = 1×10^{-4} cm, r the rate of *I* formation at 502°C = 0.8 μmol/g s, with a density of zeolite of 1.1 g/cm^3, c the reactive concentration in the gas phase = 3.1 μmol/cm^3 and a D_{eff} of 2.6×10^{-9} cm^2/s (40) a Thiele modulus (Φ_s) of 1.3×10^{-2} is obtained. The value of D_{eff} is unknown, however, a value at ambient temperature of 2.6×10^{-9} cm^2/s has been obtained by Kärger and Michel (40). This Φ_s value is so small (according to the kinetic order of the reaction) that diffusion can not contribute significantly to kinetic processes (39b). Since the value of D_{eff} will even be higher at higher temperatures (such as reaction temperatures) the value of Φ_s will even be lower. These calculations suggest that internal diffusion does not contribute significantly to kinetics described here.

H. *Kinetic Order for Isobutylene Formation*

Figure 8 shows a plot of the rate of I formation at 500°C versus partial pressure of total *n*-butenes for two different values of TOS. Curves B and C represent a B/Al-BETA

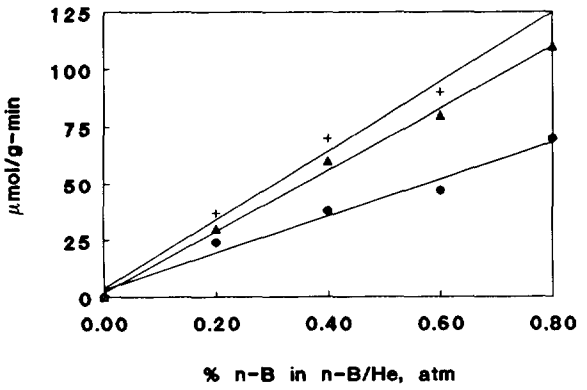

FIG. 8. Plot of activity (μmol/g · min) of isobutylene, B/Al-BETA vs partial pressure of *n*-butene. (△) 72 h TOS, (●) 74 h TOS and, (+) aged catalyst (74 h TOS) spiked with H_2O.

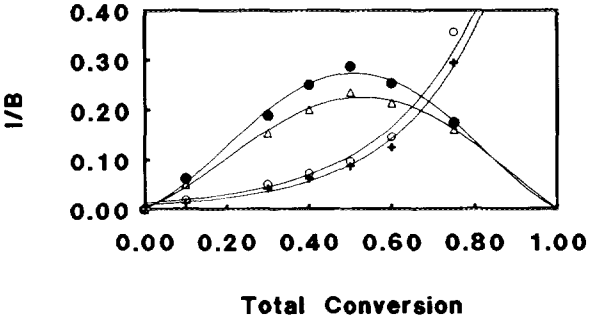

FIG. 9. Plot of isobutylene selectivity vs total conversion for B/Al-BETA zeolite: (●) isobutylene selectivity, 20% *n*-butene feed; (△) isobutylene selectivity, 70% *n*-butene feed; (○) C_3H_6 selectivity, 70% *n*-butene feed; and (+) C_3H_6 selectivity, 20% *n*-butene feed.

catalyst treated for 72 h TOS and the same material reacted for 2 more hours for a total of 74 h TOS, respectively, in a 20% B1/He feed using a differential reactor with a conversion <10%. In both cases, a straight line is obtained which shows that $\partial I/\partial t$ is first order in *n*-butenes. Similar data are observed for B/Al–ZSM-5 and B/Al–ZSM-11. Assuming that each *n*-butene produced isobutylene in a first-order reaction, the rate of isobutylene (*I*) formation will be

$$\partial[I]/\partial t = k_1[B1] + k_2[B2C] + k_3[B2T]. \quad [2]$$

Assuming the same rate constant for each step, i.e., $k_1 = k_2 = k_3 = k$, this gives:

$$\partial[I]/\partial t = k([B1] + [B2C] + [B2T]) = k[B], \quad [3]$$

which is the same as the observed experimental law.

The second major product after I is propylene. The kinetic order for the formation of propylene from n-butenes is 3/2. A straight line is obtained by plotting the rate of formation of propylene versus $P_B(3/2)$ with P_B (the total pressure of *n*-butene).

I. Selectivity to Isobutylene Versus Total n-Butene Conversion

Figure 9 (●) shows a plot of selectivity to I defined as $Y = [I]/[B_0]$ (B_0 = initial [butene]) versus total conversion $\{X = ([B_0] - [B])/[B_0]\}$ ranging from 0 to 1) for B/Al-BETA zeolite at 523°C for a feed of 20% B1/He. The maximum value of Y for *I* is 0.29 obtained for a total conversion X of *n*-butenes of 0.5. At this point, almost half of the *n*-butenes produce byproducts, the majority of which is propylene. The slope near $X = 0$ is about 0.62 and the slope near $X = 1$ approaches a value of 1. Figure 9 (△) shows a similar curve but represents a feed of 70% B1/He. The maximum yield of *I* is lower than that observed for 20% B1 with a maximum total *n*-butene conversion (X) occurring at 0.52. The slope at X = 0 is 0.47 and for $X = 1$ approaches −1. Figures 9 (○) and (+) represent conversion of C_3H_6 for the 20% B1 and 70% B1 feeds, respectively. Similar trends are observed for B/Al–ZSM-5 and B/Al–ZSM-11.

J. Selectivity to n-Butenes during Isobutylene Conversion

Isomerization of *I* to *n*-butenes has been studied using similar experimental conditions described above for *n*-butene isomerization by using a 20% *I*/He feed with a B/Al-BETA catalyst. Figure 10 gives the selectivity of *n*-butene ($[B]/[I_0]$) versus total conversion (X) of *I* $\{([I_0 - [I])/[I_0]\}$. These data show a value of Y of 0.46 at a total conversion of I of 0.58. The slope for a value of X near 0 is 1 and for X at 1 approaches −1. These data suggest that during *n*-butene isomerization to *I* that *n*-butenes (not *I*) are responsible for the formation of byproducts.

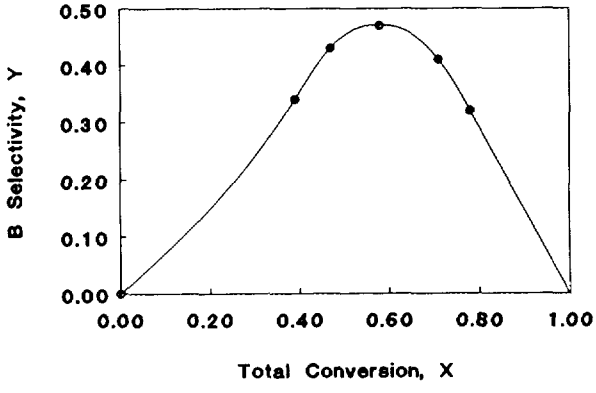

FIG. 10. Plot of *n*-butene selectivity vs total conversion for B/Al-BETA zeolite, 20% I/He feed, 523°C.

K. Other Kinetic Data

1. Hydrogen production during isobutylene formation. The production of H_2 during *n*-butene conversion over B/Al-BETA zeolite was recorded using a mass spectrometer instead of the FID. About 0.9 μmol/g min H_2 is produced for a rate of *I* formation of 86.5 μmol/g min. These data suggest that there is no direct correlation between the *I* and H_2 products. The low value for H_2 formation suggests that this product comes from dehydrogenation steps during the formation of byproducts. In order to show that H_2 does not have a significant effect during I formation, a reactive mixture of 20% B1/20% H_2/He was used. No change in rate of *I* formation was observed under these conditions with respect to non-H_2 containing feeds. These data suggest that H_2 does not participate in *I* formation or in *n*-butene transformations.

2. Effect of the presence of water during n-butene conversion. At a reaction temperature of 523°C for B/Al-BETA catalyst, a switch was made between two reactive mixtures: (20% B1/He) and (20% B1/H_2O/He) with water saturated at 18°C. The rate of I formation increases from 28.8 μmol/g min to 32.4 μmol/g min on spiking the catalyst treated for 74 h shown in Fig. 8, Curve C with water (Curve A of Fig. 8). This enhanced rate of formation of *I* can be explained by an increase in the number of Brønsted sites of the solid due to the dissociation of H_2O on Lewis sites. This is verified by monitoring the IR spectrum.

3. Regeneration of the catalyst. Figure 6 shows that these boroaluminosilicate catalysts deactivate slowly at a constant temperature. After several hours of TOS, the rate of production of *I* at 523°C using 20% B1/He with B/Al-BETA is 22 μmol/g min. The feed was then switched to 1 atm H_2 (30 cc/min) and CH_4 production was monitored using an MS. A decreasing exponential profile was recorded with an initial rate of CH_4 formation of 4 μmol/g min. The total quantity of CH_4 formed after 75 min is 8.9 μmol/g. After this treatment, the initial rate of production of *I* at 523°C using a 20% B1/He feed is 24.9 μmol/g.

After the treatment in H_2 and a purge with He, the catalyst has been treated in a 5% O_2/Ar environment (20 cc. min) at the same temperature. The total quantity of CO_2 detected by MS is 633 μmol/g after 4 h treatment (CO_2 is still produced at a low rate). After this treatment followed by 10 min He purge, the initial rate of formation of I at 523°C is 98.9 μmol/g min. Therefore, the removal of 633 μmol/g of carbon increases the rate from 24.9 to 98.9 μmol/g min. This suggests that the absorbed species which deactivate one site contain 5–6 carbon atoms (assuming an even distribution of carbon on the surface). Similar regeneration data were observed for B/Al-ZSM-5 and B/Al-ZSM-11.

TABLE 2

Comparison of Conversion, Selectivity (*S*), and Yield (*Y*) for Various ZSM-5 Catalysts

Catalyst	Temp. (°C)	Conv. (%)	*I*–*S* (%)	*I*–*Y* (%)
B-ZSM-5	600	5.8	9.8	0.6
Al-ZSM-5	560	55.8	36.9	20.6
B/Al-ZSM-5	523	58.9	49.1	28.9

Note. $[Al^{3+}]$ = 200–300 ppm for both Al-ZSM-5 and B/Al-ZSM-5.

4. Comparison of borosilicates, aluminosilicates, and boroaluminosilicates. A summary of conversions and selectivities for B-ZSM-5, B/Al-ZSM-5 and Al-ZSM-5 is given in Table 2. Enhanced selectivity to I is observed for the B/Al-ZSM-5 system. Similar results were observed for the ZSM-11 and BETA systems.

Figure 11 shows TPD data for Al^{3+}-free B-ZSM-5 zeolites that has been dehydrated at 500°C, treated with ammonia at room temperature, and evacuated overnight at 120°C. The same procedure was used to study chemisorption of pyridine and the resultant material shows two different bands near 1540 and 1460 cm^{-1}.

IV. DISCUSSION

A. Synthesis and Characterization of B Zeolites

Earlier data (29) of bulk analytical and XRD data show that B/Al-ZSM-5 and B/Al-ZSM-11 zeolites having trace amounts of Al^{3+} are crystalline. Similar data for B/Al-BETA are reported here. Al^{3+}-free materials as the B-ZSM-11 material shown in Fig. 2 can also be prepared, although particle sizes are smaller than materials with Al^{3+} impurities. EDX data of Fig. 3 do not show any Al^{3+} impurity ions in these samples. All these data are consistent with literature reports (8–15, 33, 34, 38, 41, 42).

FTIR data for B/Al-ZSM-5 of Fig. 4 show a B–O stretch at 1385 cm^{-1} and a Si–O–B skeletal vibration near 960 cm^{-1}, consistent with earlier FTIR reports (10, 12,

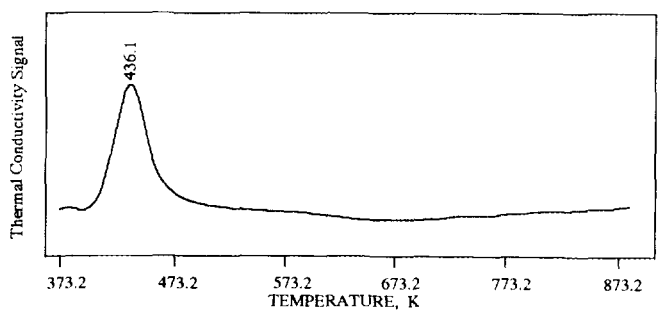

FIG. 11. Temperature-programmed desorption data for NH_3 on B/Al-ZSM-5.

16). These peaks do not shift very much for B/Al–ZSM-11. There is no clear observation of trigonal B^{3+} as has been detected near 860 cm^{-1}, although this may be below limits of detection of our apparatus. Earlier NMR and luminescence data (29) for similar samples do show trigonal boron as samples are calcined, thermally treated, or treated with acid.

B. Acid Sites

FTIR data for B/Al–ZSM-5, B/AL–ZSM-11, and B/Al-BETA after chemisorption of pyridine show the presence of both Lewis and Brønsted sites (29), at least for B/Al–ZSM-5. The TPD data for B/Al–ZSM-11 zeolites calcined at temperatures of 600, 700, 800, and 900°C (Fig. 5) clearly show a decrease in amount of desorbed NH_3 as was the case for B–ZSM-5 zeolites reported earlier (29). These data agree with our suggestion from XPS, luminescence, and NMR data (22) that B^{3+} migrates from the lattice to the surface when temperatures near 900°C are used for thermal treatment.

Catalytic and treatment studies below perhaps 700°C need to be done to avoid destruction of acid sites, although strengths of sites generated from high temperature calcination may afford materials with different acidity than for the *n*-butene isomerization catalysts reported here (vide infra). Boroaluminosilicate zeolites are known to have weak acid sites (15–28).

The ammonia TPD data of Fig. 11 and pyridine chemisorption experiments for Al^{3+}-free B–ZSM-5 suggest that B–ZSM-5 has very weak acidity due to the presence of both Brønsted and Lewis acidity. The temperature maximum for the ammonia TPD of B–ZSM-5 is at least 10°C lower than for the corresponding B/Al–ZSM-5 catalyst materials indicating much weaker acidity. The same trends have been observed for Al^{3+}-free B–ZSM-11 and B-BETA materials with respect to B/Al–ZSM-11 and B–Al-BETA catalyst (43).

C. Kinetic Studies

Due to the large number of byproducts, it is difficult to propose an accurate mechanism to explain *n*-butene conversion into *I*. However, a simple formal mechanism for *I* formation can be proposed.

We note that the kinetic order for the formation of isobutylene is 1 with respect to *n*-butenes and this suggests that the rate constants for the formation of *I* from the individual B1, B2C, and B2T are of the same orders of magnitude. The first-order rate law can be explained by the Langmuir–Hinshelwood model. For example, the rate of formation of *I* is proportional to the coverage of each *n*-butene (B1, B2C, or B2T), for B1 $\theta_{B1} = \gamma_{B1}P_{B1}/(1 + \lambda_{B1}P_{B1})$ with λ_{B1} the adsorption coefficient with P_{B1} the partial pressure of 1-butene. At the high temperatures needed for reaction to occur, $\lambda_{B1}P_{B1} < 1$ and the coverage (θ) is proportional to the partial pressure. The rate of formation of *I* is first order in B1. The same treatment can be applied to B2C and B2T so that one finally obtains the following:

$$\partial[\mathrm{I}]/\partial t = k_1P_{B1} + k_2P_{B2C} + k_3P_{B2T}. \quad [4]$$

Assuming $k_1 = k_2 = k_3$, a first-order reaction is obtained for the partial pressure of *n*-butenes:

$$\partial[\mathrm{I}]/\partial t = kP_B. \quad [5]$$

The study of conversion of *I* to *B* shows that the formation reaction of *I* is reversible. The comparison of data from Figs. 9 and 10 suggests that only *n*-butenes produce byproducts because *I* can be converted with a high selectivity to *n*-butenes even at a conversion of 0.5. The production of H_2 during isomerization and the introduction of H_2 in reactant mixtures shows that neither a hydrogenation nor a dehydrogenation step participate significantly in the formation of *I*.

Taking the above remarks under consideration, the formal mechanism

$$\mathrm{B} \underset{k_7}{\overset{k_6}{\rightleftharpoons}} \mathrm{I} \quad [6]\ [7]$$

$$\mathrm{B} + \mathrm{B} \xrightarrow{k_8} \text{By-product} \quad [8]$$

is proposed, with first-order reactions [6] and [7] and unknown order for reaction [8]. From this model and the experimental data of Fig. 9, experimental data can be compared to theoretical curves (vide infra).

The rate of formation of *I* is

$$\partial[1]/\partial t = k_6P_B - k_7P_I. \quad [9]$$

The rate of disappearance of *B* is

$$-\partial[\mathrm{B}]/\partial t = k_6P_B + k_8P_B^n - k_7P_I. \quad [10]$$

Using the definitions of selectivity to isobutylene (Y) and total conversion (X) defined above for conversion of *B* to *I*, and considering that $P_B/P_0 = [\mathrm{B}]/[\mathrm{B}_0]$ it can be shown that

$$\partial Y/\partial X = [k_6(1 - X) - k_7Y)]/ [k_6(1 - X) + k_8P_0^{n-1}(1 - X)^n - k_7Y]. \quad [11]$$

This expression shows that for the curve that $Y = f(X)$ and:

the slope at $X = 0$ is $1/[1 + (k_8P_0^{n-1}/k_6)]$,
the slope at $X = 1$ is -1,
and that at the maximum $k_7/k_6 = (1 - X)/Y$.

A comparison between these parameters and the experimental data of Fig. 9 shows the following:

(a) Experimentally, the slope (s) approaches 1 when X approaches 1 as predicted for the two initial values of P_0.

(b) From the maximum: $k_7/k_6 = 1.7$ using the curve with $P_0 = 20\%$ B/He feed and $k_7/k_6 = 1.8$ using the curve with $P_0 = 70\%$ B/He. These two values are in good agreement.

(c) The expression of the slope at $X = 0$ gives

$$k_8/k_6\, P_0^{n-1} = [(1/s) - 1],$$

and for two values of P_0 it follows that

$$[(1/s) - 1]/(1/s') - 1] = (P_0/P_0')^{n-1}.$$

Using the experimental data of Fig. 9, the order of reaction [8] is found to be $n = 1.48$ or 3/2. Note that this value is the kinetic order found for C_3H_6 production (the second major product for B conversion). Reaction [8] probably is responsible for the production of propylene.

The same kinetic model may be used for the conversion of *I* to *B* according to the reaction

$$\mathrm{I} \underset{k_{13}}{\overset{k_{12}}{\rightleftharpoons}} \mathrm{B} \qquad [12]\ [13]$$

$$\mathrm{B} + \mathrm{B} \xrightarrow{k_{14}} \text{By-product.} \qquad [14]$$

According to the rate of disappearance of *I* and the rate of formation of *B* it follows from the relationships of Y and X described above *for the conversion of I to B* that

$$\partial Y/\partial X = [k_{13}(1 - X) - k_{12}Y - k_{14}\, P_{I_0}^{n-1}\, Y^{n-1}]/[k_{13}(1 - X) - k_{12}Y]. \qquad [15]$$

A comparison of Eq. [15] [$Y = f(X)$] to the data of Fig. 10 suggests that $Y = f(X)$ and that:

(a) the slope at $X = 0$ is 1 as observed experimentally;

(b) the slope at $X = 1$ is either -1 if $n - 1 > 0$ or infinite if $n - 1 < 0$. The experimental data show that the slope approaches -1 if X approaches 1 so $n - 1 > 0$ agrees with the value of $n = 3/2$ found using results of *n*-butene conversion;

(c) at the maximum,

$$(k_{13}/k_{12})\,(1 - X_m)\,(-Y - k_{14}/k_{12})\, P_{I_0}^{n-1}\, Y_m^{n-1} = 0.$$

Using $k_{14}/k_{12} = 0.6/P_0^{n-1}$ with $P_0 = 20\%$ B/He from Fig. 10 and considering the values at the maximum $X_m = 0.58$ and $Y_m = 0.46$ with $P_{I_0} = 20\%$ *I*/He, the ratio $k_{13}/k_{12} = 2.1$ which is in good agreement with the value 1.7/1.8 found using the *n*-butene conversion data.

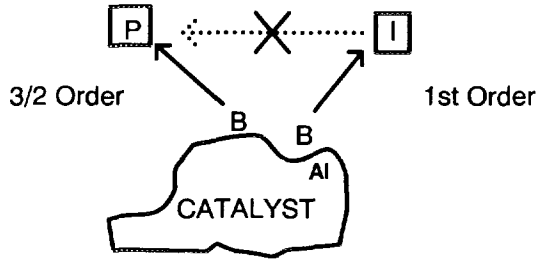

FIG. 12. Proposed model for *n*-butene isomerization with boron zeolite catalysts. P, polymer product, and I, isobutylene product.

The comparisons of experimental and theoretical data and the simple kinetic model described above show that the model is a good representation of the experiment. This means that reaction [8] is representative of the conversion of *n*-butene to the various heavier hydrocarbons that are each detected at low concentration levels.

The formation of these heavy hydrocarbons from *n*-butene explains the limit in selectivity toward I when conversion is increased. Since the reaction order of 1 for *I* seems to be maintained even at high conversion when the formation of C_3H_6 and other heavier hydrocarbons is enhanced, this suggests that the sites for the formation of I and heavier hydrocarbons are different.

D. Overview

The similarity of performance of B/Al–ZSM-5, B/Al–ZSM-11 and B/Al-BETA zeolites as regards activity, selectivity and stability implies that the structure of the zeolite is not a primary factor in the transformation of n-B to I. Different particle sizes and zeolites produce few changes suggesting again that external diffusion does not dominate. The composition of the zeolite is clearly important since Al^{3+}-free zeolites are not at all active.

On addition of Al_2O_3 binder to these materials, there is an approximate 2 fold increase in activity. These data together with the fact that B^{3+} free ZSM-5, ZSM-11, and BETA are either inactive or are primarily active for polymerization suggest a synergistic interaction between B^{3+} and Al^{3+} in these catalysts. The comparison of selectivities and conversions for B reactions over various ZSM-5 catalysts shown in Table 2 suggests that Al and B together give quite different selectivities than either B or Al alone.

A general model for the isomerization and polymerization is given in Fig. 12. It is not now apparent whether these reactions proceed over one or more sites. The fact that selectivity does not change as the catalysts are poisoned suggests that if there are multiple sites that these are poisoned equally. The fact that the surface C concentration is quite high with respect to the number of available sites suggests that poisoning is more of a physical nature

rather than chemical. FTIR of boroaluminosilicate zeolites with chemisorbed pyridine suggest that both Brønsted and Lewis sites exist on these materials. Characterization of the number of sites, their types and their roles in *n*-butene transformations are the focus of continuing research efforts (43).

V. CONCLUSIONS

The above data suggest that the reaction of B to I over boroaluminosilicate zeolites is first order in *n*-butenes; that H_2O generates Brønsted acid sites; H_2 has no effect on reaction order or rate; external diffusion occurs at low (<18 cm^3/min) flow rates; i-C_4H_8 and C_3H_6 are the major products; the reaction is 3/2 order in C_3H_6; O_2 regeneration is more efficient than H_2 regeneration; deactivation is a slow process; pure boroalites are inactive; B^{3+} and Al^{3+} interactions appear to be important; as conversion increases C_3H_6 increases; and polymer forms from *n*-butenes, and not as a secondary product from isobutylene. Kinetic modeling studies suggest that polymer production is also 3/2 order. Future studies include characterization of the number and types of sites on these catalysts (43) and attempts to control rates of isomerization and polymerization.

ACKNOWLEDGMENTS

SLS acknowledges the Department of Energy, Office of Basic Energy Sciences, Division of Chemical Sciences, for support of this research. The authors also acknowledge Texaco, Inc., for support of this research.

REFERENCES

1. Weissermel, K., and Arpe, H. J., "Industrial Organic Chemistry," p. 63. Verlag-Chemie, Weinham, 1978.
2. Szabo, J., Perrotey, J., Szabo, G., Duchet, J. C., and Cornet, D., *J. Mol. Catal.* **67,** 79 (1991).
3. Choudhary, V. R., *Chem. Ind. Dev.* **32** (1974).
4. Tabak, S. A., Krambeck, F. J., and Garwood, W. E., *AIChE J.* **32,** 1526 (1986).
5. Ono, Y., Kitagawa, H., and Sendoda, Y., *J. Chem. Soc. Faraday Trans. 1,* **83,** 2913 (1987).
6. Bhatia, T. K., and Phillips, M. J., *J. Catal.* **110,** 150 (1988).
7. J. M. Thomas, *Sci. Am.* **April,** 112 (1992).
8. Barrier, R. M., "Hydrothermal Chemistry of Zeolites," Chap. 6, p. 251. Academic Press, London, 1982.
9. Tielen, M., Geelen, M., and Jacobs, P. A., *in* "Proceedings of International Conference on Zeolite Catalysis, Siofok, Hungary, Acta. Phys. Chem. Szeged., Szeged. 1985," p. 1.
10. Vedrine, J., *in* "Zeolite Chemistry and Catalysis," (P. A. Jacobs *et al.*, Eds.), p. 25. Elsevier, Amsterdam, 1991.
11. Chu, C. T-W., and Chang, C. D., *J. Phys. Chem.* **89,** 1569 (1985).
12. Jansen, J. C., de Ruiter, R., and van Bekkum, H., *in* "Zeolites: Facts, Figures, Future" (P. A. Jacobs and R. A. Van Santen, Eds.), p. 679. Elsevier, Amsterdam, 1989.
13. Meyers, B. L., Ely, S. R., Kutz, N. A., and Kaduk, J. A., *J. Catal.* **91,** 352 (1985).
14. Scholle, K. F. M. J. G., Kentgens, A. P. M., Veeman, W. S., Frenken, P. F., and Ven der Velden, G. P. M., *J. Phys. Chem.* **88,** 5 (1984).
15. Kofke, T. J. G., Gorte, R. J., and Kokotailo, G. T., *J. Catal.* **116,** 252 (1989).
16. Chu, C. T-W., Kuehl, G. H., Lago, R. M., and Chang, C. D., *J. Catal.* **93,** 451 (1985).
17. Sayed, M. B., Aroux, A., and Vedrine, J. C., *J. Catal.*, **116,** 1 (1989).
18. Kutz, N. A., *in* "Perspectives in Molecular Sieve Science" (W. H. Flank and T. E. Whyte, Eds.), ACS Symposium Series, Vol. 368, p. 532. ACS, Washington, DC, 1988.
19. Beyer, H. K., and Borbely, G., *in* "Proc. 7th Int. Zeolite Conf." (Y. Murakami, Ed.), p. 867. Elsevier, Amsterdam, 1986.
20. Gaffney, T. R., Pierantozzi, R., and Seger, M. R., *in* "Zeolite Synthesis," (M. L. Occelli and H. E. Robson, Eds.), ACS Symposium Series, Vol. 398, p. 374. ACS, Washington, DC, 1989.
21. Sulikowski, B., and Klinowski, J., *in* "Zeolite Synthesis" (M. L. Occelli and H. E. Robson, Eds.), ACS Symposium Series, Vol. 398, p. 393. ACS, Washington, DC, 1989.
22. Taramasso, M., Perego, G., and Notari, B., *in* "Proc. 5th Int. Conf. on Zeolites, 1980," (L. V. C. Rees, Ed.), Heydon: London, p. 40.
23. Barrer, R. M., and Freund, E. F., *J. Chem. Soc. Dalton Trans.*, 1049 (1974).
24. Howden, M. G., *Zeolites* **5,** 334 (1985).
25. Coudurier, G., Auroux, A., Vedrine, J. C., Farlee, R. D., Abrams, L., and Shannon, R. D., *J. Catal.* **108,** 1 (1987).
26. Auroux, A., Sayed, M. B., and Vedrine, J. C., *Thermochim. Acta* **93,** 557 (1985).
27. Cornarao, U., and Wojchiechowski, B. W., *J. Catal.* **120,** 182 (1989).
28. Wendlandt, K. P., Unger, B., and Becker, K., *Appl. Catal.* **66,** 111 (1990).
29. Simon, M. W., Nam, S. S., Xu, W. Q., Suib, S. L., Edwards, J. C., and O'Young, C. L. *J. Phys. Chem.* **96,** 6381–6388 (1992).
30. O'Malley, P. J., and Dwyer, J., *J. Chem. Soc. Chem. Commun.*, 72 (1987).
31. Bennett, C. O., and Suib, S. L., *Catal. Today* **15,** 503 (1992).
32. Ono, Y., Kitagawa, H., and Sendoda, Y., *J. Chem. Soc. Faraday Trans. 1* **83,** 2913 (1987).
33. Kokotailo, G. T., Chu, P., Lawton, S. L., and Meier, W. M., *Nature* **275,** 119 (1978).
34. Tamarasso, M., Manara, G., Fattore, V., and Notari, B., U.S. Patent 4,656,016 (Apr. 7, 1987).
35. Jacobs, P. A., DeClerk, L. J., Van Damme, L. J., and Uytterhoven, J. B., *Trans. Faraday Soc.*, 1545 (1974), and references therein.
36. Gerberich, H. R., and Hall, W. K., *J. Catal.* **5,** 99 (1966).
37. Strull, D. R., Westrum, E. F., and Sinke, G. C., "The Chemical Thermodynamics of Organic Compounds." Wiley, New York, 1969.
38. Harrison, I. D., Leach, H. F., and Whan, D. A., *Zeolites* **7,** 21 (1987).
39. (a) Satterfield, C. N., "Heterogeneous Catalysis in Industrial Practice," 2nd ed., Chap. 11. McGraw–Hill, New York, 1991; (b) "Mass Transfer in Heterogeneous Catalysis." MIT Press, Cambridge, MA, 1970.
40. Kärger, J., and Michel, D., *Z. Phys. Chem. Leipzig* **257**(5), 983 (1976).
41. Thomas, J. M., and Williams, C., *in* "Chemical Reactions in Organic and Inorganic Constrained Systems," (R. Setton, Ed.), p. 49. Reidel, Dordrecht, 1986.
42. Scholle, K. F. M. J. G., and Veeman, W. S., *Zeolites* **5,** 118 (1985).
43. Xu, W. Q., Suib, S. L., and O'Young, C. L., *J. Catal.* **144,** 285 (1993).